ChemComm

Ultrafast Proton-Assisted Tunneling Through ZrO2 in Dye-Sensitized SnO2-core/ZrO2-Shell Films

Journal:	*ChemComm*
Manuscript ID	CC-COM-05-2018-004189.R1
Article Type:	Communication

ChemComm

COMMUNICATION

Ultrafast Proton-Assisted Tunneling Through ZrO_2 in Dye-Sensitized SnO_2-core/ZrO_2-Shell Films

Received 00th January 20xx,
Accepted 00th January 20xx

DOI: 10.1039/x0xx00000x

www.rsc.org/

John R. Swierk,[a,*] Nicholas S. McCool,[b] Jason A. Röhr,[a] Svante Hedström,[a†] Steven J. Konezny,[a,*] Coleen T. Nemes,[a] Pengtao Xu,[b] Victor S. Batista,[a,*] Thomas E. Mallouk,[b,c,*] Charles A. Schmuttenmaer[a,*]

Core-shell architectures are used to modulate injection and recombination in dye-sensitized photoelectrochemical cells. Here, we demonstrate that exposing SnO_2-core/ZrO_2-shell films to acid permits photoinduced electron transfer through ZrO_2-shells at least 4 nm thick. A novel mechanism of charge transfer is proposed where protonic defects permit ultrafast trap-assisted tunneling of electrons.

A paramount challenge in all photoelectrochemical systems for solar energy conversion is facilitating desired charge transfer events while suppressing undesired charge transfer pathways. One highly successful strategy for charge management is the use of thin, conformal surface coatings, typically deposited via atomic layer deposition (ALD).[1-3] In the case of water-splitting dye-sensitized photoelectrochemical cells (WS-DSPECs), conformal metal oxide shells can retard recombination of injected electrons and surface-bound holes.[4-6]

We recently explored the ultrafast injection dynamics of a dye-sensitized SnO_2-core/TiO_2-shell architecture for use in WS-DSPECs.[7] The TiO_2-shells were prepared on SnO_2 nanoparticle films using ALD. We used time resolved terahertz spectroscopy (TRTS) to observe either: A) Tunneling from the dye excited state directly into the SnO_2 core when the TiO_2 thickness was 6 Å or less, or B) Electron injection into the TiO_2 layer followed by trapping, and then followed by relaxation into the SnO_2-core when the TiO_2 thickness exceeded 6 Å. TRTS probes changes in oxide conductivity by monitoring ultrafast (fs–ns) photoinduced changes in THz radiation. Mobile conduction band electrons attenuate THz radiation, and thus, an increase in conductivity related to free-carrier generation manifests as a decrease in transmitted THz radiation, while a loss of mobile carriers by trapping or recombination results in an increase of transmitted THz light. Dempsey and coworkers[8] as well as Papanikolas and coworkers[9] observed similar behavior using nanosecond and ultrafast transient absorption, respectively, and also confirmed that recombination slowed with increasing shell thickness.

During our studies of SnO_2/TiO_2 films, we prepared SnO_2-core/ZrO_2-shell films as a control to distinguish between direct tunneling to the core and injection into the shell-material conduction band. Unlike TiO_2, the conduction band minimum (CBM) of ZrO_2 lies significantly above the S_1 and T_1-excited states of Ru(II)phos (Bis(2,2′-bipyridine)(4,4′-diphosphonato-2,2′-bipyridine)ruthenium(II) bromide) (*vide infra)*, which prohibits electron transfer via the ZrO_2 conduction band.[10] Contrary to our expectations, using TRTS, at pH 1 (0.1 M $HClO_4$) we observed photoinduced electron transfer into the SnO_2-core through ZrO_2-shell thicknesses of at least 40 Å (Figure 1). As expected, we observed rapid injection into bare SnO_2, as well as with 1 and 2 Å of ZrO_2 where tunneling is expected. The increase in injection amplitude with thin layers of ZrO_2 is consistent with our previous observations, which we ascribe to passivation of non-mobile SnO_2 surface states.[7,11] Beyond 2 Å of ZrO_2, however, we continue to observe significant electron injection into SnO_2, despite direct tunneling through the ZrO_2 being unrealistic (*vide infra*). We also cannot distinguish ultrafast features that can be ascribed to mobile electrons in the ZrO_2. This suggests that electron transport through the ZrO_2 must occur through non-mobile, localized states within the ZrO_2.

To gain a better sense of the manner in which electron transfer dynamics change with increasing ZrO_2 shell thickness, the TRTS traces were fit using a triple-exponential function (Equation S1) shown in red in Figure 1, and the fitting parameters are summarized in Table S1. Surprisingly, in all cases, the fast (~2 ps) and intermediate (15–20 ps) injection components are nearly unaffected by film thicknesses. The ZrO_2 shell seems to primarily affect the slowest injection component, increasing its lifetime by about a factor of 2.

[a] *Department of Chemistry and Energy Sciences Institute, Yale University, 225 Prospect Street, P.O. Box 208107, New Haven, Connecticut, 06520-8107, United States*
[b] *Department of Chemistry, The Pennsylvania State University, University Park, Pennsylvania 16802 United States*
[c] *Department of Biochemistry and Molecular Biology and Department of Physics, The Pennsylvania State University, University Park, Pennsylvania 16802 United States*
† *Current address: Department of Physics, Albanova University Center, Stockholm University, 10691 Stockholm, Sweden*
Electronic Supplementary Information (ESI) available. See DOI: 10.1039/x0xx00000x

Overall, the average weighted time constant for the electron to transit through the ZrO_2 shell increases by only a factor of ~3 for the thickest ZrO_2 shells relative to the thinnest ones. In comparison, a 25 Å thick TiO_2 layer slows the electron transfer time by an order of magnitude.[7]

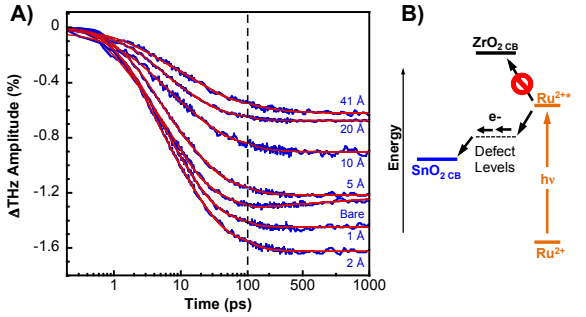

Figure 1. A) Time-resolved THz spectroscopy (TRTS) electron injection profiles monitored to 1000 ps following photoexcitation at 400 nm of Ru(II)phos-sensitized bare SnO_2 and SnO_2-core/ZrO_2-shell (1–41 Å) films in 0.1 M $HClO_4$ (aq). Solid red lines are fits of Equation 2. Dynamics from 0–100 ps are presented on an X-axis log scale while dynamics from 100–1000 ps are presented on a linear scale. B) Schematic energy level scheme for dye-sensitized SnO_2-core/ZrO_2-shell films used in TRTS measurements.

ALD has been widely utilized to deposit uniform, conformal coatings of various oxides materials, including ZrO_2 on high surface area supports.[12] Figure S1 clearly shows that the ZrO_2 shell is intact and approximately 40 Å thick after the TRTS measurements, which eliminates the possibility of ZrO_2 dissolution and dye redeposition playing roles in the electron transfer. Dye desorption is also not observed. Additionally, ALD is well established as a conformal technique, and with 40 pulses of Zr, pinholes are not expected and are highly unlikely to account for the significant injection amplitude. The TRTS traces in Figure S2 also demonstrate that mobile electrons in the SnO_2 are not photogenerated in the absence of Ru(II)phos, ruling out a contribution from direct above-band gap excitation of SnO_2 or ZrO_2

The simplest model for the injection process from the photoexcited dye through the ZrO_2 shell to the SnO_2 core is tunneling, but is shown here to be implausible. Using a band gap estimate for monoclinic ZrO_2 of 5.4 eV and a valance band offset with silicon of 3.5 eV, we can infer that the CBM of ZrO_2 lies at −1.35 V vs NHE at pH 1.[13] The structurally relaxed excited states T_1 and S_1 of Ru(II)phos have calculated potentials of 1.71 and 2.10 eV above the ground state, respectively, whereas without structural relaxation, the potentials are 1.88 and 2.25 eV, respectively. The calculated ground-state oxidation potential in CH_3CN is 1.45 V vs NHE, and the experimentally measured potential is 1.33 V vs NHE.[14] Based on these potentials, the barrier for tunneling through ZrO_2 can vary between 1.08 eV for the structurally relaxed T_1 and 0.55 for the non-relaxed S_1. Using the WKB approximation (Equation S2), this yields tunneling transmission probabilities as a function of ZrO_2 thickness (Figure 2). This figure also includes the calculated transmission for the experimental estimate of the barrier, as well as for a hypothetical tunneling barrier of 0.01 eV that would result in the high injection rate close to what we actually observe. This clearly demonstrates that direct tunneling does not contribute significantly except for the two thinnest ZrO_2 layers of < 2.04 Å.

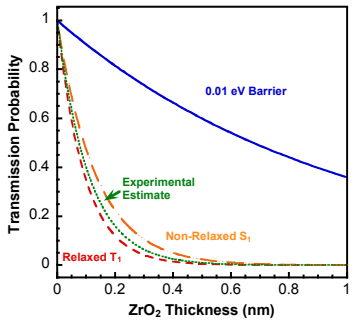

Figure 2. Tunneling probability according to the WKB approximation, Equation S2, using a barrier height corresponding to the difference between the ZrO_2 CBM and the excited state potential of Ru(II)phos. Also included is the largest hypothetical barrier (0.01 eV) that could allow for the injection through the ZrO_2.

Given that tunneling from the dye excited state into the SnO_2 conduction band is unlikely, a different mechanism of charge transport must exist. We note that in the absence of acid exposure (Figure S3), electron transport through the ZrO_2 is impeded, offering insight into the mechanism of charge transport. A possible mechanism involves trap-assisted tunneling facilitated by protonic defects (Figure 1B). Houssa and coworkers describe a protonic trap energy that lies 0.77 eV below the CBM,[15] which would be appropriately positioned to accept an electron from the S_1 state of Ru(II)phos and may be close in energy to the T_1. Transport through this defect level is consistent with our TRTS results that show the fastest injection components (possibly related to the S_1 state)[16] are only marginally slowed by varying thicknesses of ZrO_2, while the slowest component (possibly related to the T_1) is significantly more sensitive to ZrO_2 thickness. Additionally, leakage current from sub-band gap charge hopping has been observed in ZrO_2 capacitors.[17]

In an effort to gain a better understanding of how the acid treatment specifically affects the ZrO_2 layers, XPS measurements were carried out on high surface area SnO_2 nanoparticle films coated with 40 Å of ZrO_2. We investigated an as-prepared SnO_2/ZrO_2 film, a SnO_2/ZrO_2 film soaked overnight in anhydrous ethanol, and a SnO_2/ZrO_2 film soaked overnight in 0.1 M $HClO_4$. We also studied an uncoated, sintered SnO_2 film to identify any possible changes to the SnO_2 induced by soaking in solvent. Finally, as reference materials, we characterized commercial ZrO_2 and SnO_2 nanopowders. Survey scans of all films showed the presence of C, O, Zr and/or Sn, respectively. No nitrogen or chlorine was observed with high-resolution XPS scans of the N 1s and Cl 2p region.

Figure S5a and Figure S5b show high-resolution XPS scans of the Zr 3d and O 1s edge regions, respectively. Figure S6 shows high-resolution scans of the C 1s and Sn 3d regions. All of the XPS peaks were referenced to adventitious carbon at 284.4 eV (Figure S6c). For the SnO_2 and ZrO_2 reference samples, we observed a broad peak in the C 1s region related to adventitious carbon that can be fit with two components, while the four samples prepared from doctor-bladed pastes

displayed an additional peak at 288.4 to 288.6 eV, suggesting the sintering process fails to remove all the carbon from these films. Importantly, we do not observe any extra C 1s peaks for the acid-treated SnO_2/ZrO_2 samples, which is an indication that carbon is not doping the ZrO_2 films.

In the Zr 3d region (Figure S5a), there is no evidence of Zr in the SnO_2 reference and sintered SnO_2 samples. For the other samples, Zr $3d_{3/2}$ and Zr $3d_{5/2}$ peaks are clearly seen, and there is an additional feature at 186.7 eV in the ZrO_2 reference sample. This feature is most likely related to surface suboxide species.[18] The Zr $3d_{3/2}$ peaks at 184.1–184.5 eV and Zr $3d_{5/2}$ peaks at 181.6–182.1 eV are related to crystalline ZrO_2 species.[19] The X-ray diffraction pattern in Figure S7 demonstrates that the ZrO_2 reference sample the monoclinic phase, which is the most stable polymorph at room temperature.[20] It is clear from Figure S5a that the Zr 3d peaks at 184.4 and 182.0 eV for the ZrO_2 reference, as-prepared, and ethanol-treated SnO_2/ZrO_2 samples line up well, suggesting the as-prepared ZrO_2 ALD films are monoclinic after heating.

In Figure S5a it is also apparent that the Zr peaks in the $HClO_4$-treated sample shift to higher binding energies of 184.6 and 182.2 eV. It is unlikely that a phase change has occurred because, in the presence of strong acid and/or strain, the tetragonal phase of ZrO_2 undergoes a spontaneous phase transformation to monoclinic at room temperature.[21,22] Instead we assign this shift to the incorporation of protons into the ZrO_2 shell. Chen et al.[23] observed a shift in the Nb 3d spectrum to higher binding energies upon hydrogen incorporation into Nb_2O_5, while electrochromic Nb_2O_5 films charged with Li^+ exhibit a similar shift in the Nb 3d spectrum.[24] Shim and coworkers have found that hydrogen impurities introduced during the ALD deposition of yttria-stabilized zirconia results in a shift to higher energy of the Y 3d peaks.[25]

This assignment is further supported by the O 1s spectra (Figure S5c). The O 1s XPS spectrum for monoclinic ZrO_2 is composed of two components: bridging oxygen (530.1 eV) and –OH groups (~531 eV).[26] For the as-prepared and ethanol-treated SnO_2/ZrO_2 samples we find that the ratio of –OH groups to bridging oxygen is about 0.52, while in the $HClO_4$-treated sample the ratio is 0.7 (Figure S5c). Introduction of protons into ZrO_2 is thought to induce breaking of bridging oxygen bonds to form ZrOH,[27] consistent with our results.

To gain further insight into the mechanisms of transport, 4 and 20 nm films of ZrO_2 were deposited on planar Al_2O_3 and patterned with gold electrodes. As shown in Figures 3a and S8 (inset), the current–voltage (I–V) curve for the as-prepared ZrO_2 thin film exhibits an extremely small current response on the order of femtoamps and hysteresis consistent with a large RC time constant. This originates from the high dielectric constant and resistivity of native ZrO_2. Direct exposure to 0.1 M $HClO_4$ (Figure 3b) results in a ~10 order of magnitude increase in conductivity after just three hours. A similar increase in conductivity is also observed in 4 nm films after overnight exposure to acid (Figure S8a).

To understand whether acid treatment primarily affects the surface or bulk material, we fabricated three devices in series on a single 20 nm ZrO_2 film by depositing patterned gold electrodes (Figure 3c), leaving exposed ZrO_2 "troughs" between each of the evaporated gold films. Without any acid treatment, the current across all three devices was on the order of ten femtoamps (Figure 3a), indicative of the high resistivity of the as-prepared ZrO_2 films. Device 1 was treated with 0.1 M $HClO_4$ for three hours by adding the acid to the first device well. This allowed us to expose a single partition of the ZrO_2 film to $HClO_4$ without exposing the other areas. The acid was subsequently removed, and the current across all three devices was measured. The current in device 1 reproducibly increased by ~10 orders of magnitude, consistent with a substantial increase in conductivity. The current in device 2 was also observed to reproducibly increase by two orders of magnitude. After three hours, there was no increase in the current in device 3, however, after 9 hours of acid treatment of device 1, we did observe a factor of 20 increase in the current across device 3. The fact that the current increased in devices 2 and 3 despite not being directly exposed to acid is an indication that the conductivity in this system is not a surface property but rather a bulk property. These results are consistent with proton incorporation into the film and subsequent diffusion through the bulk of the ZrO_2. We note that the increases in the conductivity of devices 2 and 3 are unlikely to be related to gaseous $HClO_4$ as the vapor pressure of pure $HClO_4$ is only 6.8 mmHg. In addition, Leng et al. observed a similar effect during the insulator to metal transition in tungsten oxide.[28]

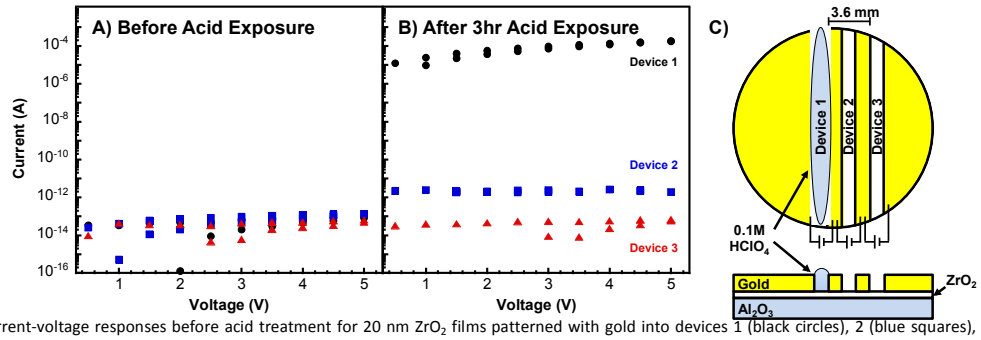

Figure 3. a) Current-voltage responses before acid treatment for 20 nm ZrO_2 films patterned with gold into devices 1 (black circles), 2 (blue squares), and 3 (red triangles). b) Current-voltage response for the same three devices after acid-treatment of device 1 for 3 hours. c) Cartoon schematic of arrangement of devices 1, 2, and 3.

In summary, we have demonstrated a novel pathway for photoinduced electron transfer through wide band gap ZrO_2. Despite direct tunneling being unphysical, our TRTS measurements demonstrate that efficient, rapid electron transport is possible through thick ZrO_2 layers. We suggest a trap-assisted tunneling mechanism via mid-gap protonic defects. Furthermore, XPS measurements demonstrate that exposure to acid results in a shift of the Zr 3d peaks consistent with proton incorporation, while the O 1s spectrum of acid-treated samples shows an increase in the relative ratio of hydroxyl oxygen to bridging oxides due to the formation of ZrOH. Exposure to acid results in at least a six order of magnitude increase in DC conductivity. Using multiple devices patterned on the same film, we present evidence of proton incoporation and transport throughout the bulk film. The results of this study offer new insights into development of functional thin films for solar energy conversion and potential strategies for inducing conductivity.

This work was supported by the Office of Basic Energy Sciences, Division of Chemical Sciences, Geosciences, and Energy Biosciences, Department of Energy, under contracts DE-FG02-07ER15911 and DE-FG02-07ER15909 as well as by a generous donation from the TomKat Charitable Trust. N.S.M. thanks the National Science Foundation for support as a graduate fellow under Grant DGE1255832. Instrumentation and facilities used in this project were supported by the Pennsylvania State University Materials Research Institute Nanofabrication Laboratory under National Science Foundation Cooperative Agreement ECS-0335765. The XPS analysis was performed at the Yale Materials Characterization Core.

Conflicts of interest

There are no conflicts to declare.

Notes and references

1 S. Hu, N. S. Lewis, J. W. Ager, J. Yang, J. R. McKone and N. C. Strandwitz, *J. Phys. Chem. C*, 2015, **119**, 24201–24228.
2 C. Du, M. Zhang, J.-W. Jang, Y. Liu, G.-Y. Liu and D. Wang, *J. Phys. Chem. C*, 2014, **118**, 17054–17059.
3 Y. Li, A. Pang, C. Wang and M. Wei, *J. Mater. Chem.*, 2011, **21**, 17259–17264.
4 S.-H. A. Lee, Y. Zhao, E. A. Hernandez-Pagan, L. Blasdel, W. J. Youngblood and T. E. Mallouk, *Faraday Discuss.*, 2012, **155**, 165–176.
5 A. Pang, X. Sun, H. Ruan, Y. Li, S. Dai and M. Wei, *Nano Energy*, 2014, **5**, 82–90.
6 B. D. Sherman, D. L. Ashford, A. M. Lapides, M. V. Sheridan, K.-R. Wee and T. J. Meyer, *J. Phys. Chem. Lett.*, 2015, **6**, 3213–3217.
7 N. S. McCool, J. R. Swierk, C. T. Nemes, C. A. Schmuttenmaer and T. E. Mallouk, *J. Phys. Chem. Lett.*, 2016, **7**, 2930–2934.
8 R. R. Knauf, B. Kalanyan, G. N. Parsons and J. L. Dempsey, *J. Phys. Chem. C*, 2015, **119**, 28353–28360.
9 M. K. Gish, A. M. Lapides, M. K. Brennaman, J. L. Templeton, T. J. Meyer and J. M. Papanikolas, *J. Phys. Chem. Lett.*, 2016, **7**, 5297–5301.
10 J. L. Lyons, A. Janotti and C. G. Van de Walle, *Microelectronic Engineering*, 2011, **88**, 1452–1456.
11 J. R. Swierk, N. S. McCool, C. T. Nemes, T. E. Mallouk and C. A. Schmuttenmaer, *J. Phys. Chem. C*, 2016, **120**, 5940–5948.
12 C. Prasittichai, J. R. Avila, O. K. Farha and J. T. Hupp, *J. Am. Chem. Soc.*, 2013, **135**, 16328–16331.
13 Y. R. Chen, P. Zhou, J. Li and L. Y. Chen, *J. Vac. Sci. Technol. B*, 2009, **27**, 1030.
14 K. Hanson, M. K. Brennaman, A. Ito, H. Luo, W. Song, K. A. Parker, R. Ghosh, M. R. Norris, C. R. K. Glasson, J. J. Concepcion, R. Lopez and T. J. Meyer, *J. Phys. Chem. C*, 2012, **116**, 14837–14847.
15 M. Houssa, M. Tuominen, M. Naili, V. Afanas'ev, A. Stesmans, S. Haukka and M. M. Heyns, *J. Appl. Phys.*, 2000, **87**, 8615–8620.
16 J. Jiang, J. R. Swierk, S. Hedström, A. J. Matula, R. H. Crabtree, V. S. Batista, C. A. Schmuttenmaer and G. W. Brudvig, *Phys Chem Chem Phys*, 2016, **18**, 18678–18682.
17 Y. Seo, S. Lee, I. An, C. Song and H. Jeong, Semicond. Sci. Technol., 2009, **24**, 115016.
18 M. Matsuoka, S. Isotani, S. Miyake, Y. Setsuhara, K. Ogata and N. Kuratani, J. Appl. Phys., 1996, **80**, 1177–1181.
19 A. Mondal and S. Ram, Chem. Phys. Lett., 2003, **382**, 297–306.
20 C. J. Howard, R. J. Hill and B. E. Reichert, Acta Cryst Sect A Found Cryst, 1988, **44**, 116–120.
21 F. Shojai and T. A. Mäntylä, J. Eur. Ceram. Soc., 2001, **21**, 37–44.
22 V. E. Annamalai, C. V. Gokularathnam and R. Krishnamurthy, J. Mater. Sci. Lett., 1992, **11**, 824–827.
23 W. P. Chen, K. F. He, Y. Wang, Y. M. Hu, J. L. Cao and H. L. W. Chan, Jpn. J. Appl. Phys., 2010, **49**, 051103.
24 N. Özer, D. G. Chen and C. M. Lampert, Thin Solid Films, 1996, **277**, 162–168.
25 K. Bae, K. S. Son, J. W. Kim, S. W. Park, J. An and F. B. Prinz, Int. J. Hydrogen Energy, 2014, **39**, 2621–2627.
26 S. Ardizzone and C. L. Bianchi, J. Electroanal. Chem., 1999, **465**, 136–141.
27 M. Houssa, A. Stesmans, M. Naili and M. M. Heyns, Appl. Phys. Lett., 2000, **77**, 1381–1383.
28 X. Leng, J. Pereiro, J. Strle, G. Dubuis, A. T. Bollinger, A. Gozar, J. Wu, N. Litombe, C. Panagopoulos, D. Pavuna and I. Božović, npj Quantum Materials, 2017, **2**, 35.

Table of Contents Figure

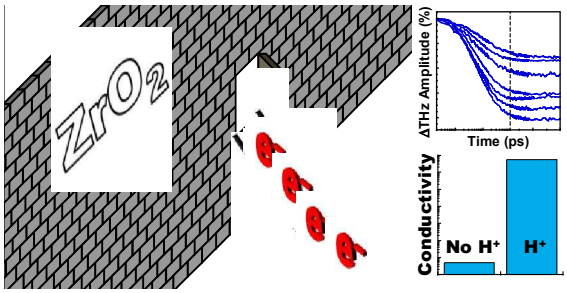

Exposing ZrO_2 to strong acid induces protonic defects that permit ultrafast electron transfer through at least 4 nm of ZrO_2.